International Journal of Engineering and Innovative Research

http://dergipark.gov.tr/ijeir

POLAR SIMULATION OF SUBSONIC FLOW AROUND NACA 4610 AIRFOIL IN HORIZONTAL AXIS WIND TURBINE

Etuk Ekom Mike[1*], Ebhojiaye Raphael Sylvester [1], Amiolemhen Patrick [1]

[1]University of Benin, Faculty of Engineering, Department of Production Engineering, Benin City, Nigeria.

[*]Corresponding Author: alwaysetuk@gmail.com
(**Received:** 06.05.2020; **Revised**: 25.05.2020; **Accepted:** 15.06.2020)

ABSTRACT: This study provide details on the characteristics of horizontal axis wind turbine airfoil under subsonic flow regime at distinct angle of attacks (AoA) using XFOIL. Using a fixed Mach number (Ma) of 1000,000 and Renolds number (Re), the XFOIL modelled cambered airfoil was simulated at various AoA including -10º, -5º, 0.0º, 5º, 10º, 15º, 22º and 25º to observe the variations in lift, drag, lift and drag coefficient and their effects on the overall wind turbine performance. It was observed that constant increase in AoA can prevent separation in airflow while continuous reduction in AoA can make airflow separation more pronounce, thereby, causing decrese in the rate at which the lift coefficient increases. A negative pitching moment coefficient was observed, indicating a nose-down moment which would reduce the angle of attack on the rotor blade. It was also found that the drag coefficient C_D varied proportionately with the AoA, and lower C_D values indicate less drag foces on the on the airfoil. The results indicated that the lift to drag ratio initially increase as the AoA increases upto a maximum point of 108.64, but as the AoA is increased further, the L/D ratio decreases until the stalling angle is reached. In summary, the rotor blade undergoes minimum drag at fairly low AoA while the lifting ability of the rotor is quite low at low AoA.

Keywords: Wind Turbine, Blade Foil, Drag Force, Aerodynamics, Lift Force, Renolds Number

1. INTRODUCTION

To achieve full range of optimal operating condition in a wind turbine blade, robust numerical and computational approach is required in addition to the design calculations. The outcome can be validated by comparing with experimental data for accuracy of results [1]. According to Bertagnolio et al. [2], experimental measurement and/or flow field simulation of airfoils are used as the basis for evaluating the aerodynamic behaviour of wind turbine blades. Alrobaian et al. [3] designed and fabricated a low cost open typed subsonic compressible flow wind tunnel and the flow field measured as wall pressure reading indicated a stable flow at Mach number of 0.6, 0.7, 0.8 and 0.9 respectively. Moreover, with approximately 80% area, the exit velocity was found to be constant. Winslow et al. [4] examined NACA 0009 and NACA 0012 airfoils for drag and lift performance as well as surface pressure and flow field characteristics. The result revealed that below Re of 10^6, lift and drag characteristics were difficult to be assumed optimum or better but below Re of 10^5, the cambered airfoils had better lift and drag characteristics. Arun and Surya [5] designed a horizontal axis wind turbine with two different airfoil sections including the straight and swept back pattern using QBlade. The straight blade design produced 250KW of power at peak wind speed of 36m/s while the swept back bade produced 310 KW of power at peak wind speed of 40m/s, indicating that the swept back blade design outperformed the straight blade pattern. Mohokar and Kale [6] employed QBlade in the

optimization of a wind turbine chord length. This was experimented on ten different blade designs by changing their chord lengths between the range of 30 and 120 mm at a fixed wind velocity of 11.5 m/s, and the result revealed that at 90 mm chord length, maximum power coefficient was obtained. Gantasala et al. [7] Numerically Investigated the Aeroelastic behaviour of a wind turbine with iced blades using FAST software. The outer third of the blade produced over 50% of the turbine's total power and severe icing in this part of the blade reduced the power output and aeroelastic damping of the blade's flapwise vibration modes. Increase in the blade mass due to ice lead to reduction in its natural frequencies. Symmetrical icing of the blades reduced the loads acting on the turbine components while asymmetrical icing of the blades induced loads and vibrations in the tower, hub, and nacelle assembly at a frequency synchronous to rotational speed of the turbine. Etuk et al. [8] examined the normal, radial, axial and tangential loading cycles undergone by wind turbine rotor blades and their effects on the displacement of the blade structure using QBlade finite element sub module. Geometry of the deformed blades were characterized by twisting and bending configuration at maximum strain deformation at frequencies up to 200 Hz. From the deflection values obtained, it was found that normal loading cycle would cause the highest level of structural damage on the rotor blade followed by radial, axial and tangential loading. The aim of this study is to provide an open source turbine calculation that is seamlessly integrated into XFOIL, an airfoil design and analysis tool/software. The motivation for this is to create a one solution for the design and aerodynamic computation of wind turbine blades. The integration in XFOIL enables the user to rapidly design custom airfoils and compute their polars, extrapolate the polar data to a range of 360^{o}, and directly integrate them into a wind turbine simulation. By so doing, the procedures of exporting and importing foil and geometry data between different programs is avoided as well as the troubles involved. At the same time, the integration of the BEM and DMS code into XFOIL's sophisticated GUI will make this software accessible to a huge number of wind related applications without the usual command line interface software tools.

2. METHODS

The software XFOIL is programed to analyse and compute the flow around subsonic isolated airfoils. It is a software used for the calculation of profile polars. The polars were generated starting from alpha = -10 in first a negative direction up to 25 in a positive direction. For the design a NACA 4610 foil was used. An efficient wind rotor blade has many airfoil profiles blended at an angle of twist terminating at a circular flange. The airfoil parameters are presented in Table 1.

Table 1. NACA 4610 airfoil Design parameters.

Parameter	Value (%)	At (%)
Thickness	10	29
Camber	4	59.5
Points	99	
TE_{flap} (Deg)	0.00	
TE_x (Deg)	0.00	
TE_y (Deg)	0.00	

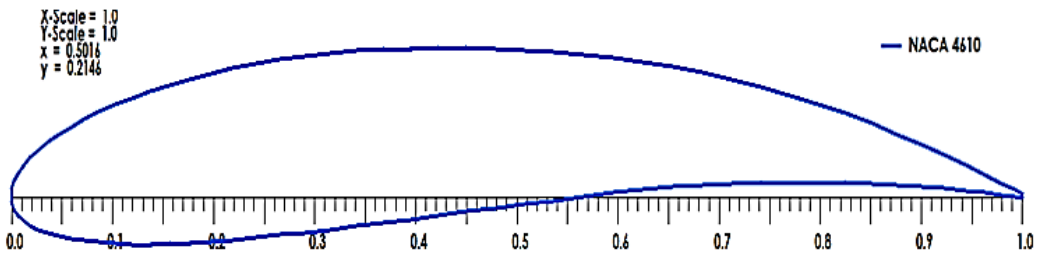

Figure 1. Diagram of the Blade Foil.

As shown in Figure 2, a circular foil with a drag coefficient of 1.2 was used for the root of the blade to enhance the blade structural strength. The parameters of the root foil are presented in Table 2. This part of the blade has low relative wind velocity as a result of its relatively small rotor radius but however carries the highest load [9]. The low wind velocity results in reduced aerodynamic lift, leading to large chord lengths. With this, the blade profile becomes excessively large at the rotor hub to enable it support the weight of the blade as well as the loads encountered during rotation.

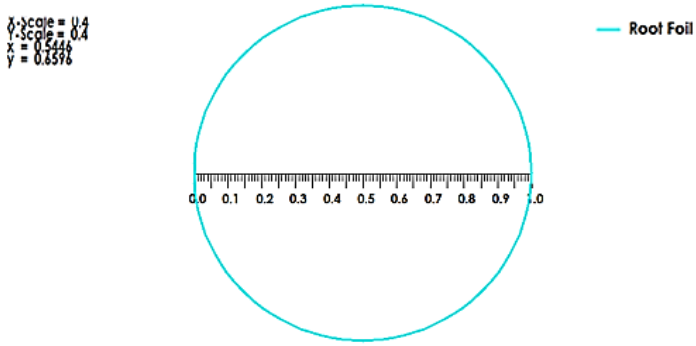

Figure 2. Airfoil for root of Blade.

Table 2. NACA 4610 root foil Design parameters.

Parameter	Value (%)	At (%)
Thickness	100	50
Camber	-0.00	99.90
Points	101	
TE_{flap} (Deg)	0.00	
TE_x (Deg)	0.00	
TE_y(Deg)	0.00	

The forces acting along the length of the blade s_i are obtained by $(p_i\text{-}p_0)s_i$. The lift (L) force and the drag (D) force per unit with of the blade alongside all the forces acting on the drag and lift direction can be obtained by integrating as follows:

$$L = \sum(p_{1-}p_0)s_1 * sin(\theta_1 + \alpha) \quad (1)$$

$$D = \sum(p_{1-}p_0)s_1 * cos(\theta_1 + \alpha) \quad (2)$$

Were p_1 and p_0 are the pressure points on the airfoil, θ is the angle of inclination against the blade chord and α is the angle of attack.

The lift and drag coefficient is given by Equation 3:

$$C_L = \frac{L}{(1/2)\rho U^2 c} \quad (3)$$

$$C_D = \frac{D}{(1/2)\rho U^2 c} \quad (4)$$

Where L is the lift force, D is the drag force, c is the chord length, ρ is the air density and U is the mainstream velocity. Pitching moment coefficient plays a vital role in understanding the principles of aerodynamic centre of an airfoil, and it is given by Equation 5:

$$C_m = \frac{M}{qSc} \quad (5)$$

The Reynolds number is given by Equation 6;

$$Re = \frac{cU}{v} \quad (6)$$

Where M is the pitching moment, q is the dynamic pressure, S is the wing area, c is the chord length of the airfoil and *v* is the kinematic viscosity of air. The local pressure coefficient which is the difference between local static pressure and free-stream static pressure is given by Equation 7.

$$C_p = \frac{P - P_\infty}{\frac{1}{2}\rho_\infty U_\infty^2} \quad (7)$$

The total or stagnation upstream pressure which is the sum of the static and dynamic pressure at that point according to Bernoulli's equation is given by Equation 8;

$$P_T = P + \frac{1}{2}\rho_\infty U_\infty^2 \quad (8)$$

In terms of differential pressures, C_p can be written in the expression in Equation 9. In this case, C_p at the airfoil stagnation point is equal to unity [10].

$$C_p = \frac{P - P_\infty}{P_T - P_\infty} \quad (9)$$

2.1. Xfoil Design Module

The software is adequate for teaching, as it provides a 'hands on' feeling for HAWT and VAWT rotor design and shows all the fundamental relationships and concepts between twist, chord, foils, turbine control and the power curve in an easy and intuitive way. The GUI serves as a post processor to conducted rotor simulations as well and gives deep insight into all relevant blade and rotor variables for verification, to compare different rotor configurations, or even to study the numerical algorithm and the dependencies among the aerodynamic variables. In addition to that, the software at hand is flexible and user-friendly for wind turbine blade design. Hence, it can also act as a modular system for future implementations that can exploit the possibilities that a combination of manual and parametric airfoil design and analysis coupled with a blade design and simulation tool offers. The functionality of the BEM software includes the following features:

i. extrapolation of XFOIL generated or imported polar data to 360^o AoA
ii. advanced blade design and optimization, including 3D visualization, using XFOIL generated or imported profiles
iii. computation of wind turbine performance over wind speed range
iv. manual selection of BEM and DMS correction algorithms
v. manual selection of all relevant simulation parameters
vi. data browsing and visualization as post processing
vii. export functionality for all created simulation data

3. RESULTS AND DISCUSSION

During revolution which occurs at an angle of 360^o, a wind turbine blade experiences much higher angles of attack than the wing of an airplane. For stall-regulated wind turbines, the flow phenomenon is even used as a means to limit the power produced. As stall is generally avoided in aerodynamics, the coefficients corresponding to high AoA are not of interest and therefore not available. Additionally, AoA in the post stall range may occur temporarily during the airfoil iteration procedures.

The lift and drag coefficients consequently have to be extrapolated for the whole 360^o range of the AoA. In general, experimental pre-stall data ($\alpha \cong 15$) is available for common air foils and XFOIL is suitable to generate such data as well. For post stall data on the other hand, some further considerations are needed. With increasing AoA, the frontal area facing the airflow increases, too. As stall occurs, the foil dramatically stops producing lift, and the drag coefficient increases. Around 180, the trailing edge of the streamlined air foil faces the flow resulting in decreasing drag and higher lift again. Hence, the flow characteristics evolve from those of a thin, streamlined air foil to those of a blunt body and back during a 180 revolution of the blade. Polar that are either imported or as a result of an XFOIL analysis, can be extrapolated to the full 360^o AoA range in the 360^o polar extrapolation sub module.

Wind turbines are usually denoted by the wind speed across the rotor blade section relative to the speed of sound. This is therefore the air speed ratio to the speed of sound commonly known as Mark number. For Subsonic flow, Mark no. < 0.8, transonic flow, Mark no. > 0.8 but <1.2, supersonic flow, Mark no. >1.2 but <5.0 and for hypersonic flow, Mark no. > 5.0. The Mark number designated by QBlade sofware for the purpose of the simulation carried out in this study was 0.020 which falls within the specified range of values for subsonic flow. The difference in Mark number is due to the relative importance of compressible effects which can be neglected in subsonic flows but plays a vital role in the aforementioned flows. For subsonic flows, the air density is almost constant but decreasing the cross sectional area can result in increase in the flow velocity and decrease in pressure. Likewise increasing the area can result can result in decrease in the flow velocity and increase in pressure. However for higher speeds above subsonic range, some of the energy of the turbine rotors compresses the air and locally changes the air density. The compressibility effect alters the amount of resulting force on the rotors and becomes more pronounced as the speed increases near and beyond the speed of sound (330 m/s or 760 mph). As a result, small disturbances in the flow are transmitted to other parts of the wind turbine isentropically or with constant entropy but a sharp disturbance can generate shock waves that affects the aerodynamics (lift and drag) of the rotor blade.

Figures 3-10 represent results obtained from the polar simulation of the horizontal axis wind turbine blade at various degrees of Alpha. As shown in Figures 3-10, the simulated blade profiles were done using QBlade software which evaluated the blade profile and graphically

assigned a generated scale depending on the value representing the Alpha for each blade profile. In other words, the value representing Alpha (α) at each blade simulation phase is the angle of attack that determines the minimum, optimum and maximum drag or lift force. Table 3 shows summary of the polar simulation results extracted from the blade simulation profiles at different angles of attack.

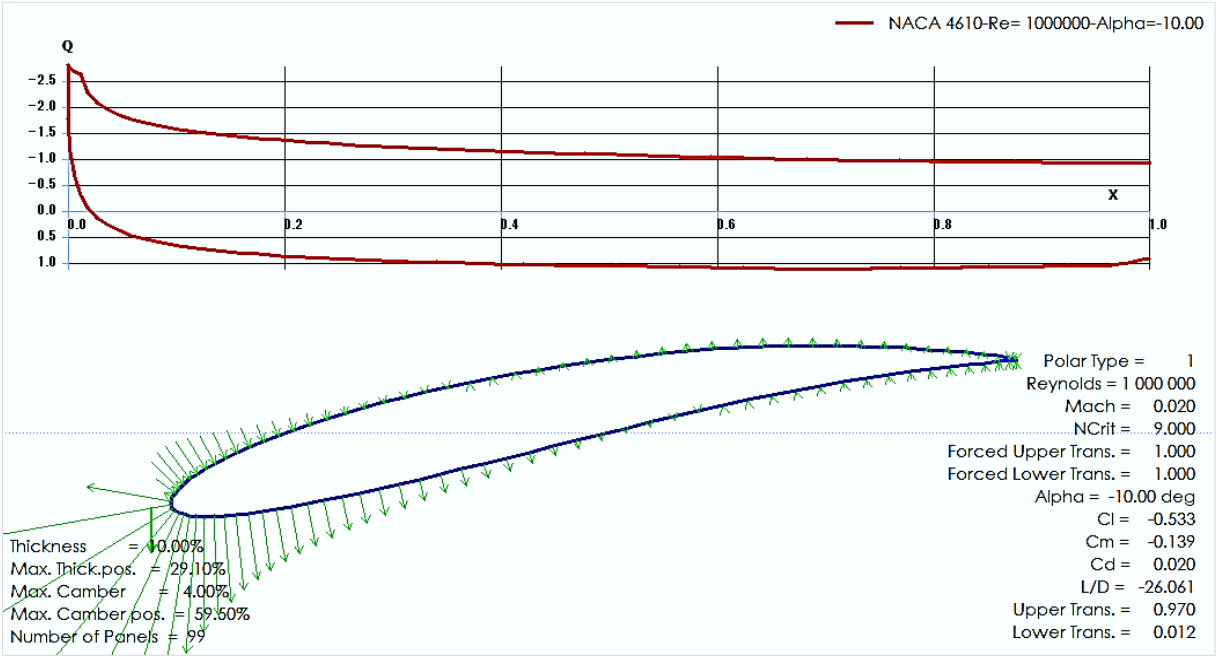

Figure 3. Blade Simulation Profile for AoA of -10 deg.

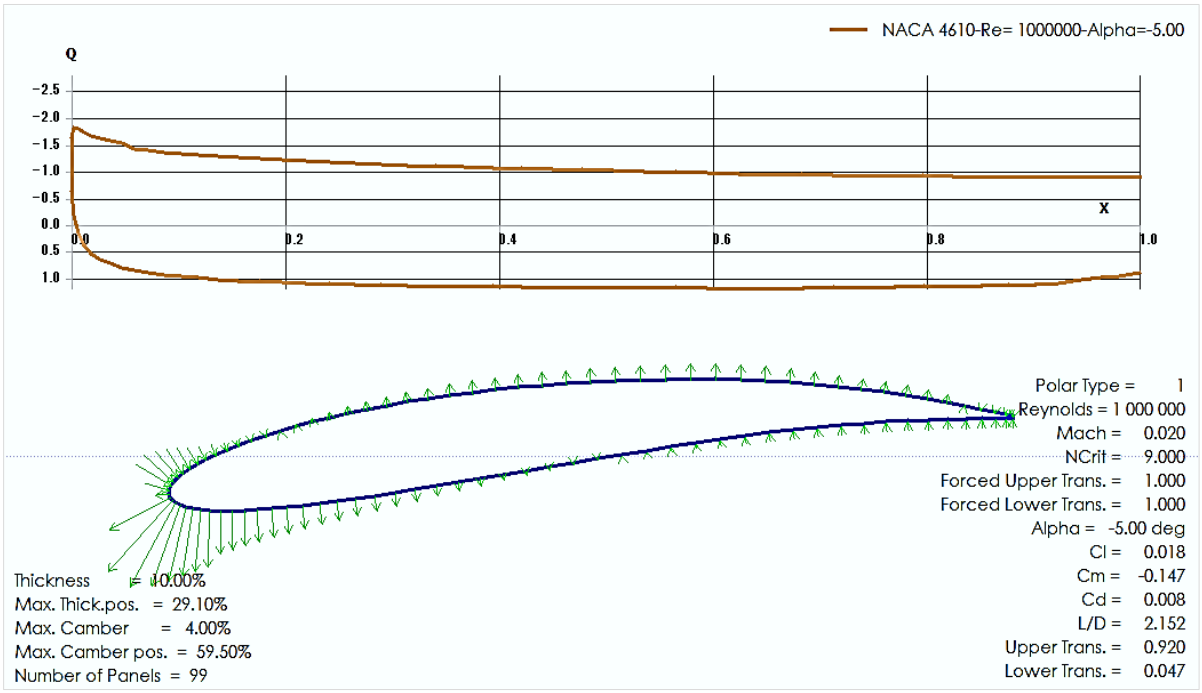

Figure 4. Blade Simulation Profile for AoA of -5.00 deg.

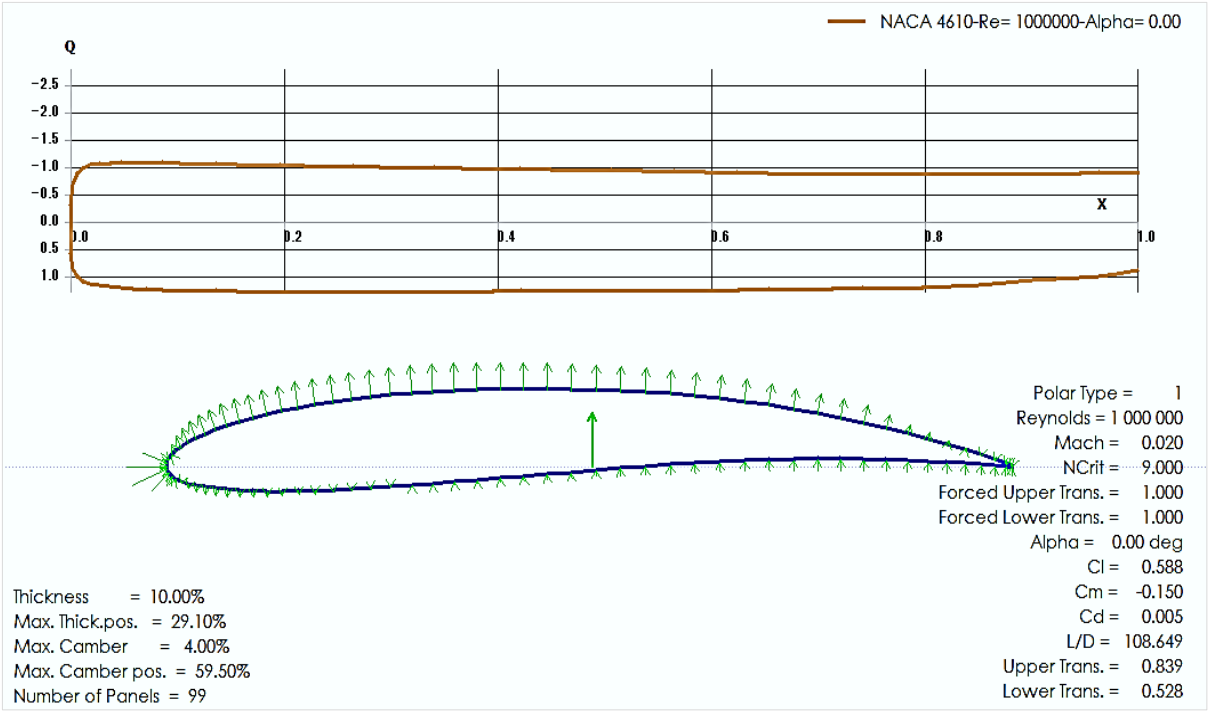

Figure 5. Blade Simulation Profile for AoA of 0.00deg.

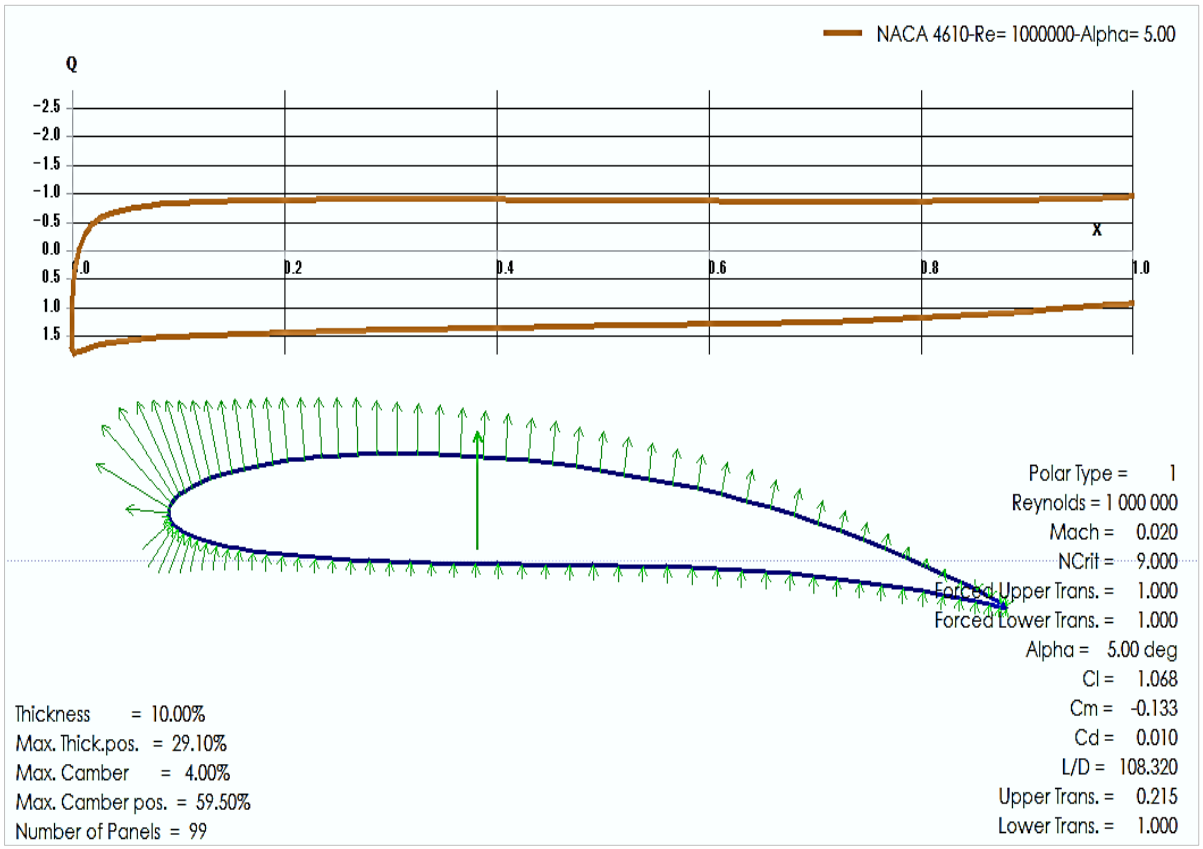

Figure 6. Blade Simulation Profile for AoA of 5.00deg.

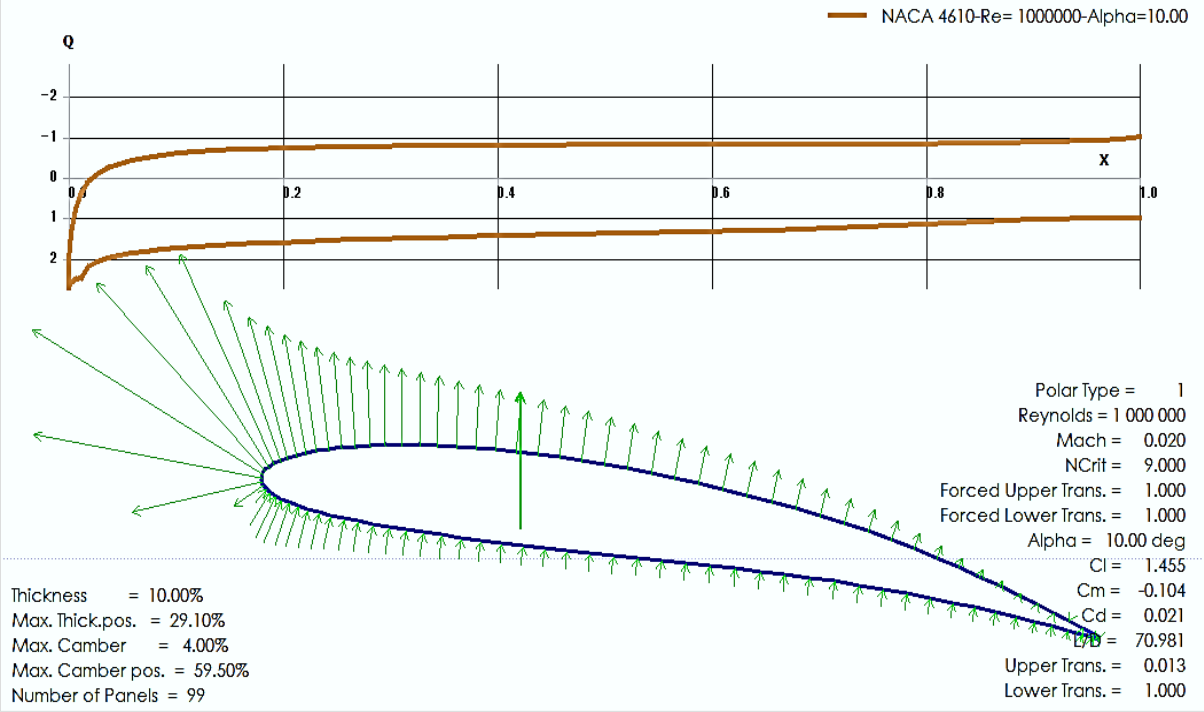

Figure 7. Blade Simulation Profile for AoA of 10.00deg.

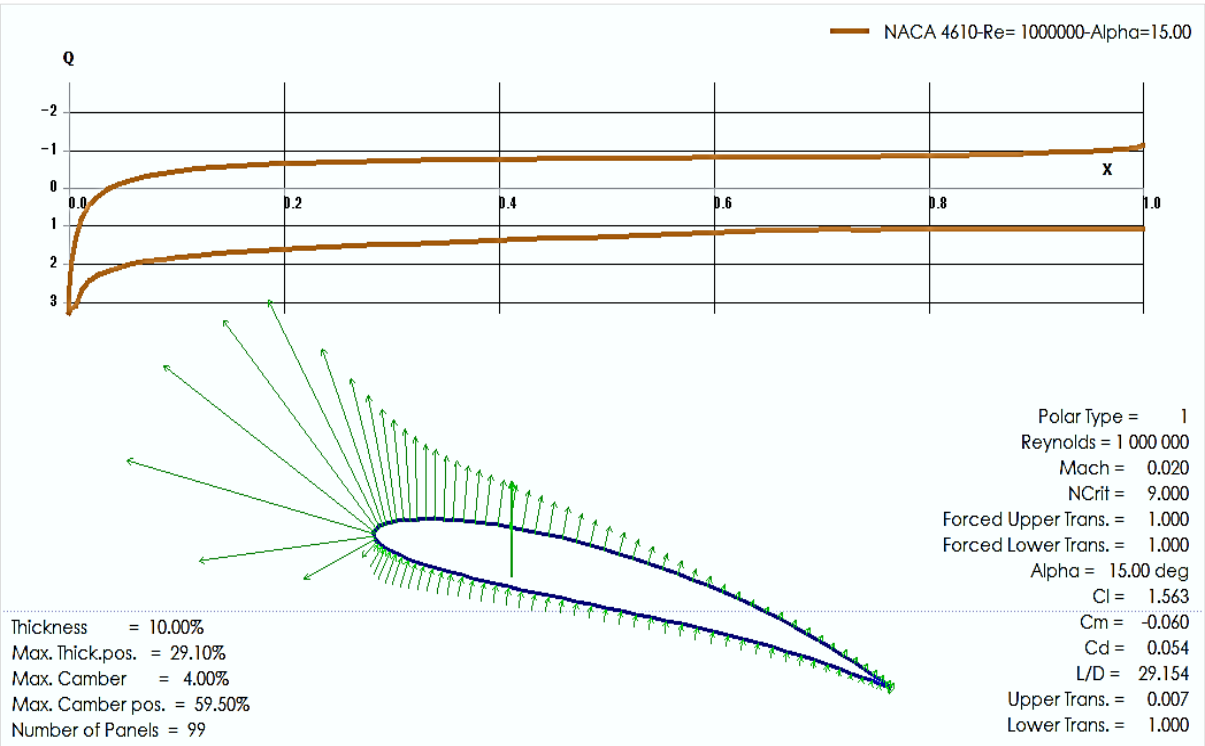

Figure 8. Blade Simulation Profile for AoA of 15.00deg.

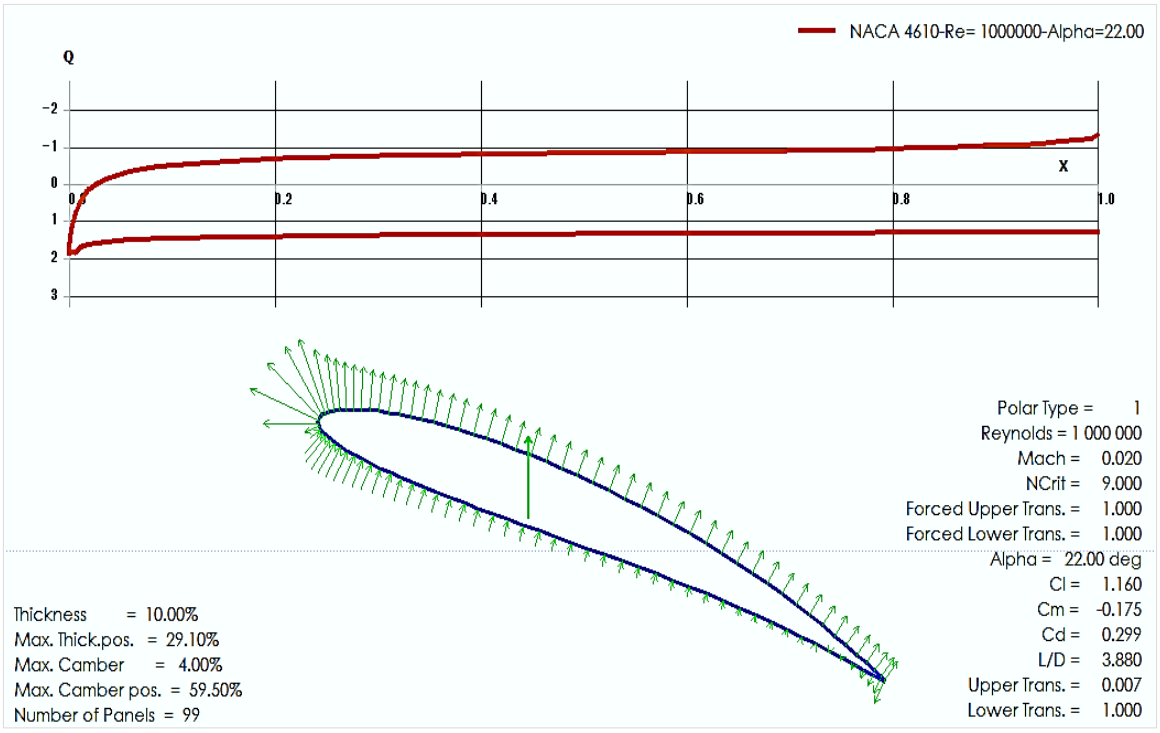

Figure 9. Blade Simulation Profile for AoA of 22deg.

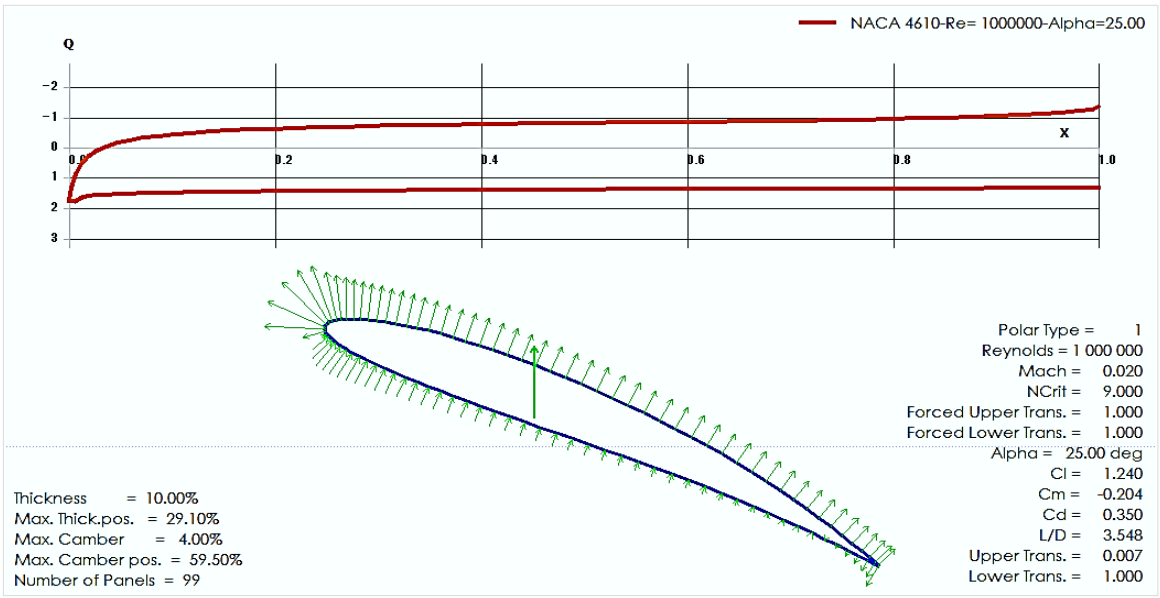

Figure 10. Blade Simulation Profile for AoA of 25.00deg.

Table 3. Summary of the Polar Simulation Results.

Alpha (deg)	Cl	Cm	Cd	L/d
-10	-0.533	-0.139	0.02	-26.061
-5	0.018	-0.147	0.008	2.152
0	0.588	-0.15	0.005	108.649
5	1.068	-0.133	0.01	108.32
10	1.455	-0.104	0.021	70.981
15	1.563	-0.06	0.054	29.154
22	1.16	-0.175	0.299	3.88
25	1.24	-0.204	0.35	3.548

Angle of attack (AoA) increases with increasing lift coefficient up to a certain maximum point, after which, the lift coefficient decreases and varies with increasing angle of attack. This can be observed in Figure 11, where the lift coefficient increases from -0.5 to a maximum point of 1.5 at AoA of 15^{o} before reduction begins to occur. There was no separation of airflow in this case as the angle of attack increased continuously through the simulation. However, reduction in angle of attack indicates that separation of airflow from the upper surface of the blade becomes more pronounce, resulting in decrease in the rate at which the lift coefficient increases. The AoA which produces the highest lift coefficient is referred to as the critical angle of attack also known as the stall angle of attack. In operating conditions below the critical angle of attack, as the angle of attack decreases, the lift coefficient also decrease. Similarly above the critical angle of attack, as the angle of attack increases, the smoothness of airflow over the surface of the airfoil begins to lessen and the air begins to separate from the airfoil surface. Generally on most airfoil geometries, as the angle of attack increases, the flow separation point on the upper surface of the airfoil shifts from the trailing edge towards the leading edge. Hoverer, at critical angle of attack, separation in the upper surface flow is more pronounced and the airfoil produces its maximum lift coefficient, and further increase in the AoA can cause the upper surface flow to become fully separated with further reduction in the lift confident.

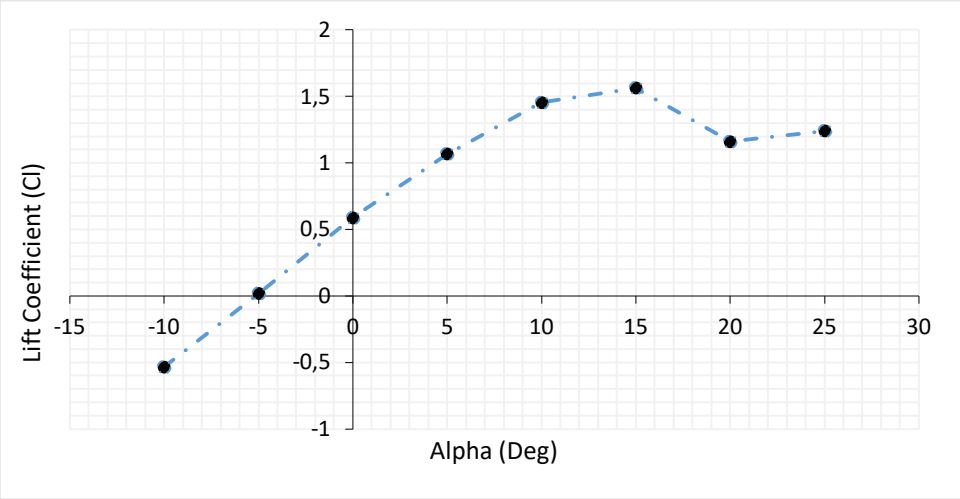

Figure 11. Graph of Lift Coefficient against Alpha.

Figure 12 represents a graph of pitching moment coefficient (Cm) against angle of attack. As graphically demonstrated in Figure 12, a negative pitching moment coefficient indicates a nose-down moment which reduces the angle of attack of the rotor blade in the absence of a control input. Such occurrence is of great advantage in the sense that the wind turbine may resort to a condition in the linear lift region (stable) rather than the stall or post stall region (unstable). In aerodynamics, the pitching moment on an airfoil is the moment or torque produced by the aerodynamic force acting on the airfoil when the aerodynamic force is considered to be acting on the aerodynamic centre of the airfoil rather than on the centre of pressure. By convection, the pitching moment is considered to be positive when it is found pitching the airfoil in the nose-up direction. However, conventional cambered airfoils supported at the aerodynamic centre pitch nose-down, causing the pitch moment coefficient of the airfoils to be negative like in the case presented in Figure 12. Camber represents the asymmetry between the two surfaces of an airfoil, with the upper surface of the airfoil usually being more convex (positive camber). It is commonly designed into an airfoil to minimize its lift coefficient which in turn minimizes the stalling speed of the wind turbine. Aerodynamic centre is the point on a chord line of the airfoil at which the pitching moment coefficient does not vary with AoA.

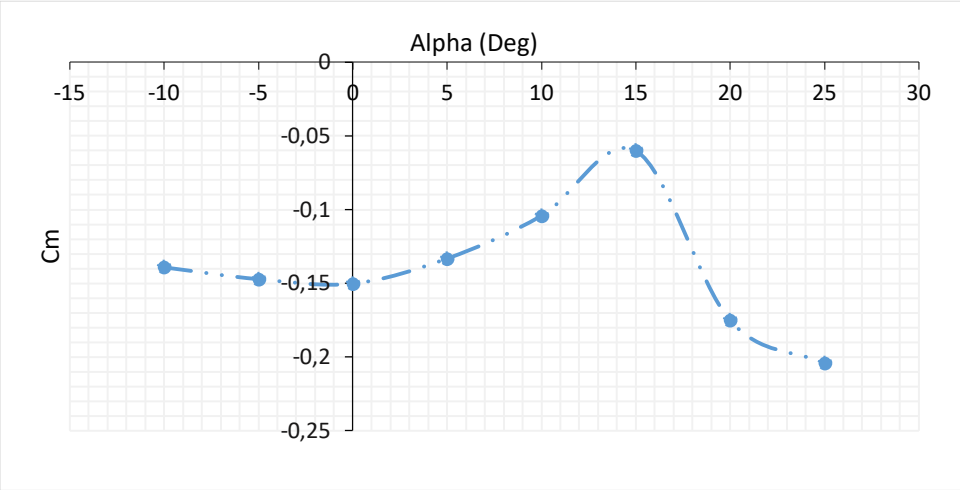

Figure 12. Graph of Pitching Moment coefficient (Cm) against Alpha.

Figure 13 represents a plot of drag coefficient against the angle of attack. Drag coefficient is a number that is used in modelling of complex dependencies of drag on shape, inclination as well as some conditions. It can be observed that at AoA of -10^o, drag coefficient of 0.02 is produced, and this further shows a gradual decrease such that, at AoA of 0^o, zero drag coefficient is observed. However, at AoA of 15^o and 25^o, drag coefficient of 0.054 and 0.35 are observed, indicating that the drag coefficient vary with the angle of attack. In similar study carried out by Tang et al. [11], drag coefficient of 0.058 and 0.059 were obtained for corrugated airfoil and NACA2408 airfoil at AoA of 2^o. In the context of fluid dynamics, drag is referred to as the forces acting on a solid object in the direction of relative flow, usually in opposite direction to the flow. From aerodynamic point of view, drag forces acting on a body are due to the differences in pressure and viscous sharing stresses, and are therefore classified into two (2) components namely: frictional drag (viscous drag) and pressure drag (form drag). In other words, the airfoil is considered as a streamline body (like in the case of the rotor blade understudied in this research) if friction drag (viscous drag) dominates pressure drag but when pressure drag (form drag) dominates friction drag, such a body is known as blunt body.

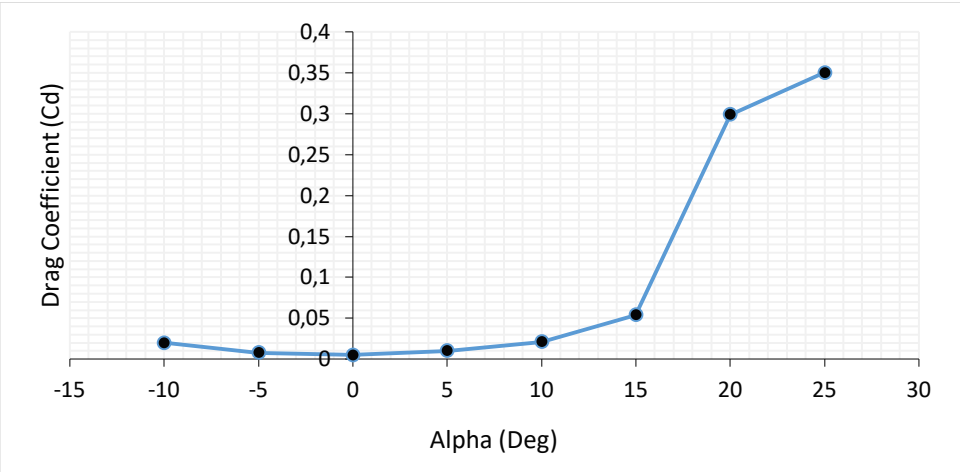

Figure 13. Graph of Drag Coefficient against Alpha.

Figure 14 represents a graph of lift to drag ratio (L/D) against angle of attack. L/D ratio in practical sense is a measure of how efficient an aerodynamic surface is generating lift force at the expense of drag force. It can be observed that at AoA of -10^o, L/D ratio of -26.061 is produced, and this further shows a sharp increase such that, at AoA of -5^o and 0^o, L/D ratio of 2.152 and 108.64 is observed. This is followed by gradual decrease such that at progressive

angle of attacks at 5º, 10º 15º and 25º, L/D ratios of 108.32, 70.98, 29.15 and 3.54 are produced in decreasing order. The sharp increase on the negative side of the plot and the gradual decline observed in the positive side of the plot indicates that the L/D ratio varies with a given angle of attack. This implies that for a normally cambered airfoil, as the AoA increases, the L/D increases rapidly to the maximum value which can be observed at 108.64, but as the AoA is increased further, the L/D ratio decreases until the stalling angle is reached and even decreases further beyond that angle. For each AoA, the L/D ratio can be calculated by dividing CL by CD (or lift by drag). By so doing, a graph representing the variation of L/D ratio as a function of AoA can be plotted.

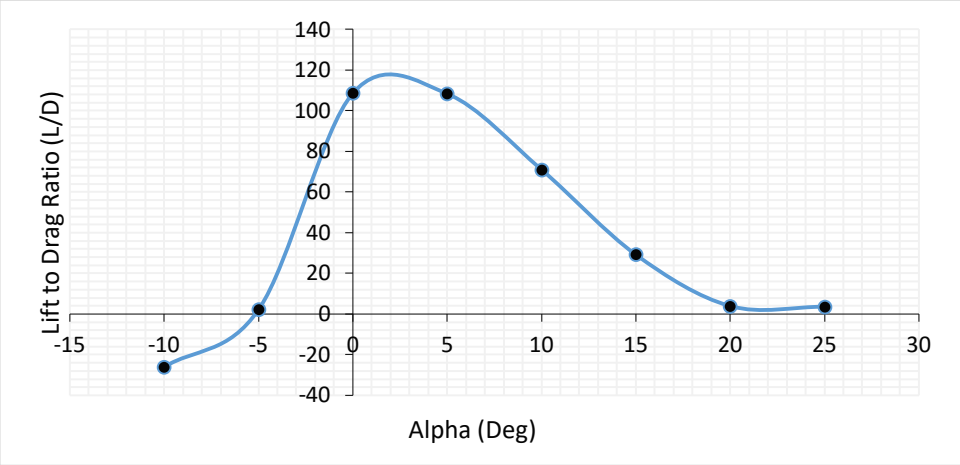

Figure 14. Graph of L/d against Alpha.

Drag polar represents the relationship between the lift and drag for wind turbine airfoils or objects exposed to fluid flow, expressed as a function of the drag coefficient dependent on the lift coefficient. Both coefficients are dependent on three (3) dimensionless variables namely: angle of attack, Reynolds number (Re) and Mach number (Ma). It may be described using mathematical equation or represented in a diagram (plotted in Figure 15) known as polar plot. While the lift coefficient increases from -0.533 to 0.588, the drag coefficient is observed to decrease from 0.02 to 0.005 as shown in Figure 15. Further increase in the C_L from 0.588, 1.068, 1.455 and 1.563 is characterized by corresponding increase in the C_D from 0.005, 0.01 and 0.021, 0.054 respectively. The C_L and C_D values represented in this plot has a specific Re and Ma (1,000,000 and 0.020) as could be seen on the rotor blade simulation profiles in Figure 3-10, but the plot itself is obtained by varying AoA (from -10 deg to 25 deg) for each simulation phase and computing the C_L and C_D. The major reason why C_L is plotted against C_D is that for a wide range of AoA variation, there is trade-off between both coefficients such that, higher CL requirement may lead to higher or lower CD depending on the AoA. In scenarios where higher CL is required, understanding how these variables are connected to each other is based on the drag polar diagram.

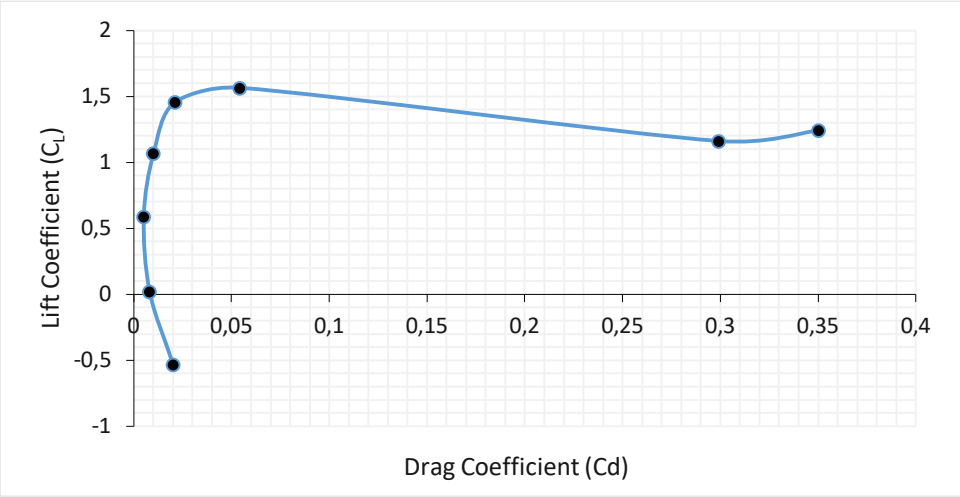

Figure 15. Graph of Lift Coefficient against Drag Coefficient.

4. CONCLUSIONS

In this study, Polar Simulation of Subsonic Flow around NACA 4610 Airfoil was successfully carried out using AIFOIL software. The cambered airfoil geometry had a specific Re and Ma (1,000,000 and 0.020) which were computed with different AoA. The simulation which considered angles of attack in the order of -10, -5, 0.0, 5, 10, 15, 22 and 25 degree indicated an increase or decrease in the lift, drag and lift to drag ratio of the rotor blade which in turn influences the aerodynamic performance in a negative or positive manner as well as the overall performance of the wind turbine. Moreover, the study also revealed that the rotor blade experiences minimum drag at fairly low AoA while its lifting capacity is also very low at low AoA. However, for selection of optimum operating data and in-depth understanding of the lift and drag characteristics at various AoA, wind turbine operators may try to simulate cambered airfoils at lower and higher Re and Ma to observe the airfoil behavior as well as the wind turbine performance.

REFERENCES

[1] Duque, E. P. N., Burklund, M. D. and Johnson, W. (2003). Navier-stoke and Comprehensive Analysis Performance Predictions of the Nrel Phase Vi Experiment. 22nd ASME Wind Energy Symposium, Reno, Nevada, USA, January, 2003. American Institute of Aeronautic and Astronauts, 2003-0355.

[2] Bertagnolio, F., Sorensen, N. N. and Rasmussen, F. (2004). New Insight into the Flow arrond a Wind Turbine Airfoil Section. Special Topic Conference, The Science of making Torque from Wind, Delft, 19-21 Aril 2004, The Netherlands.

[3] Alrobaian, A. A., Khan, S. A., Asadullah, M., Ahmed, F. and Imtiyaz, A. (2018). A New Approach to Low-cost Open-typed Subsonic Compressible Flow Wind Tunnel for Academic Purpose. International Journal of Mechanical and Production Engineering Research and Development, 8(6), 383-394.

[4] Winslow, J., Otsuka, H., Govindarajan, B. and Chopra, I. (2018). Basic Understanding of Airfoil Characteristics at Low Reynolds Numbers (104-105). Journal of Aircraft, 55(3), 1050-1061.

[5] Arun, A. K. and Surya, J. (2019). A Comparison of the Straight Blade and Swept Back Blade Horizontal Axis Wind Turbine. SSRG International Journal of Mechanical Engineering, 2348-8360, 30-35.

[6] Mohokar, A. and Kale, N. W. (2017). Development of the Performance of Small Horizontal Axis Wind Turbine Blade by Optimizing its Chord Using QBlade Software. International Journal of Advanced Engineering and Research Development, 4(11), 790-796.

[7] Gantasala, S., Tabatabaei, N., Cervantes, M. and Aidanpaa, J. (2019). Numerical Investigation of the Aeroelastic Behaviour of a Wind Turbine with Iced Blades. Energies, 12(2422), 1-24.

[8] Etuk, E. M., Ikpe, A. E. and Adoh, U. A. (2020). Design and Analysis of Displacement Models For Modular Horizontal Wind Turbine Blade Structure. Nigerian Journal of Technology, 39(1), 121-130.

[9] Schubel, P. J. and Crossley, R. J. (2012). Wind Turbine Blade Design. Energies, 5, 3425-3449.

[10] Kandil, M. A. F. and Elnady, A. O. (2017). Performance of GOE-387 Airfoil Using CDF. International Journal of Aerospace Sciences, 5(1), 1-7.
[11] Tang, H., Lei, Y., Li, X. and Fu, Y. (2019). Numerical Investigation of the Aerodynamic Characteristics and Attitude Stability of aBio-Inspired Corrugated Airfoil for MAV or UAV Applications. Energies, 12(4021), 1-25.